Dynamic and weighted stabilizations of the L-scheme applied to a phase-field model for fracture propagation

C. Engwer, I.S. Pop, T. Wick

UHasselt Computational Mathematics Preprint
Nr. UP-19-13

Dec. 15, 2019

Dynamic and weighted stabilizations of the L-scheme applied to a phase-field model for fracture propagation

Christian Engwer, Iuliu Sorin Pop, Thomas Wick

Abstract We consider a phase-field fracture propagation model, which consists of two (nonlinear) coupled partial differential equations. The first equation describes the displacement evolution, and the second is a smoothed indicator variable, describing the crack position. We propose an iterative scheme, the so-called L-scheme, with a dynamic update of the stabilization parameters during the iterations. Our algorithmic improvements are substantiated with two numerical tests. The dynamic adjustments of the stabilization parameters lead to a significant reduction of iteration numbers in comparison to constant stabilization values.

1 Introduction

This work is an extension of [3] in which an L-type iterative scheme (see [5, 8]) with stabilizing parameters for solving phase-field fracture problems was proposed. In [3], the stabilization parameters were chosen as constants throughout an entire computation. With these choices, the convergence of the scheme has been proven rigorously. The resulting approach performs well in the sense that an unlimited number of iterations compared to a truncated scheme yields the same numerical solution. The results were validated by investigating the load-displacements curves.

Christian Engwer
Institut für Numerische und Angewandte Mathematik Fachbereich Mathematik und Informatik der Universität Münster Einsteinstrasse 62 48149 Münster, Germany, e-mail: christian.engwer@uni-muenster.de

Iuliu Sorin Pop
Universiteit Hasselt, Faculty of Sciences, Agoralaan Gebouw D - B-3590 Diepenbeek, Belgium, e-mail: sorin.pop@uhasselt.be

Thomas Wick
Leibniz Universität Hannover, Institut für Angewandte Mathematik, Welfengarten 1, 30167 Hannover, Germany, e-mail: thomas.wick@ifam.uni-hannover.de

Moreover, the robustness of the scheme w.r.t. spatial mesh refinement was shown. Nonetheless, the iteration numbers (for an unlimited number of iterations) remained high.

In this work, we propose and compare two extensions of the aforementioned scheme. First, we update the L scheme parameters dynamically. Second, we use an adaptive weight depending on the fracture location inside the domain. For the latter idea, we use the phase-field variable to weight L locally.

The outline of this work is as follows: In Section 2 the model is stated whereas Section 3 presents the dynamic choice of the stablization parameters. In Section 4, we present two numerical tests to study the performance of the proposed scheme.

2 The phase-field fracture model

We consider an elliptic problem stemming from the crack propagation model proposed in [3]. $\Omega \subset \mathbb{R}^d$ is a d-dimensional, polygonal and bounded domain. We use the spaces $W^{1,\infty}(\Omega)$, containing functions having essentially bounded weak derivatives in any direction, and $H_0^1(\Omega)$ containing functions vanishing at the boundary of Ω (in the sense of traces) and having square integrable weak derivatives. $(\cdot,\cdot)$ stands for the $L^2(\Omega)$ inner product. For the ease of writing we use the notations $V := (H_0^1(\Omega))^d$ and $W := W^{1,\infty}(\Omega)$. The vector-valued displacements are denoted by u. For modeling fracture propagation in Ω, a phase field variable φ is used. This approximates the characteristic function of the intact region of Ω. Written in weak form, we solve the following problems iteratively

- **Problem 1**^{i}: Given $(u^{i-1}, \varphi^{i-1}) \in V \times W$, find $u^i \in V$ s.t. for all $v \in V$

$$a_u(u^i, v) := L_u(u^i - u^{i-1}, v) + \Big(g(\varphi^{i-1})\boldsymbol{\sigma}^+(u^i), \mathbf{e}(v)\Big) + \Big(\boldsymbol{\sigma}^-(u^i), \mathbf{e}(v)\Big) = 0. \tag{1}$$

- **Problem 2**^{i}: Given $(\varphi^{i-1}, u^i, \bar{\varphi}) \in W \times V \times W$, find $\varphi^i \in W$ s.t. for all $\psi \in W$

$$\begin{aligned} a_\varphi(\varphi^i, \psi) := {} & L_\varphi(\varphi^i - \varphi^{i-1}, \psi) + G_c\varepsilon(\nabla\varphi^i, \nabla\psi) - \frac{G_c}{\varepsilon}(1 - \varphi^i, \psi) \\ & + (1-\kappa)(\varphi^i\boldsymbol{\sigma}^+(u^i) : \mathbf{e}(u^i), \psi) + (\Xi + \gamma[\varphi^i - \bar{\varphi}]^+, \psi) = 0. \end{aligned} \tag{2}$$

In case of convergence, the first terms in the above are vanishing, and the limit pair $(u, \varphi) \in V \times W$ solves a time discrete counterpart of the model in [3], if $\bar{\varphi}$ is interpreted as the phase field at the previous time step. In this context, with $\Xi \in L^2(\Omega)$ and $\gamma > 0$, the last term in (2) is the augmented Lagrangian penalization proposed in [9] for the irreversibility constraint of the fracture propagation.

Furthermore, in the above, ε is a (small) phase-field regularization parameter, $G_c > 0$ is the critical elastic energy restitution rate, and $0 < \kappa \ll 1$ is a regularization parameter used to avoid the degeneracy of the elastic energy. The latter is similar to replacing the fracture with a softer material. Next, $g(\varphi) := (1-\kappa)\varphi^2 + \kappa$ is the degradation function, and $\mathbf{e} := \frac{1}{2}(\nabla u + \nabla u^T)$ is the strain tensor.

The stress tensor in the above is split into a tensile and compressive part,

$$\boldsymbol{\sigma}^+ := 2\mu_s \mathbf{e}^+ + \lambda_s [\mathrm{tr}(\mathbf{e})]^+ I, \quad \boldsymbol{\sigma}^- := 2\mu_s (\mathbf{e} - \mathbf{e}^+) + \lambda_s \big(\mathrm{tr}(\mathbf{e}) - [\mathrm{tr}(\mathbf{e})]^+\big) I,$$

where $[\cdot]^+$ stands for the positive cut of the argument. Further, $\mathbf{e}^+ = \mathbf{P}\boldsymbol{\Lambda}^+\mathbf{P}^T$, with $\mathbf{P}$ being the matrix containing the unit eigenvectors corresponding to the eigenvalues of the strain tensor $\mathbf{e}$. In particular, for $d = 2$ one has $\mathbf{P} = [v_1, v_2]$ and

$$\boldsymbol{\Lambda}^+ := \boldsymbol{\Lambda}^+(u) := \begin{pmatrix} [\lambda_1(u)]^+ & 0 \\ 0 & [\lambda_2(u)]^+ \end{pmatrix}.$$

3 The L-scheme with dynamic updates of the stabilization parameters

The iteration (1)-(2) is essentially the scheme proposed in [3], in which the stabilization parameters L_u and L_φ are taken constant. To improve the convergence behaviour of the scheme, we propose a dynamic update of these parameters.

Dynamic update at each iteration / constant in space: The iteration discussed in [3] uses constant parameters L_u and L_φ. With this choice, the convergence has been proved rigorously. However, the number of iterations can remain high. High iteration numbers for phase-field fracture problems were also reported in [4, 10]. To improve the efficiency, we suggest in this work to update L_u and L_φ at each iteration i:

$$L_i = a(i) L_{i-1}, \qquad \text{where } L_i := L_{u,i} = L_{\varphi,i}.$$

Inspired by numerical continuation methods in e.g. [1], one would naturally choose a large L_0 and $a(i) := a < 1$ to obtain a decreasing sequence $L_0 > L_1 > L_2 > \ldots$, updated until a lower bound L_- is reached. However, this seems not to be a good choice in phase-field fracture since the system does not have a unique solution. Consequently, with increasing i the iterations would oscillate in approaching one or another solution, and the algorithm convergence deteriorates. For this reason, we propose the other way around: the closer the iteration is to some solution, the larger the stabilization parameters is chosen, so that the iterations remain close to this solution. We choose $a(i) := a > 1$, yielding $L_0 < L_1 < L_2 < \ldots$ up to a maximal L_*.

On the specific choice of the parameters: A possible choice for a is $a(i) := 5^i$ ($i = 0, 1, 2, \ldots$), while $L_0 := 10^{-10}$. This heuristic choice and may be improved by using the solution within the iteration procedure, or a-posteriori error estimates for the iteration error. Moreover, $a(i) := 5^i$ is motivated as follows. Higher values greater than 5 would emphasize too much the stablization. On the other hand, too low values, do not lead to any significant enhancement of the convergence behaviour. We substantiate these claims by also using $a(i) = 10^i$ and $a(i) = 20^i$ in our computations.

Dynamic update using the iteration: An extension of the strategy is to adapt the L-scheme parameters in space by using the phase-field variable $\varphi^{n,i-1}$. We still take $L_i = aL_{i-1}$, but now $a := a(i, \varphi^{n,i-1})$. Away from the fracture, we have $\varphi \approx 1$ and

essentially only the elasticity component (2) is being solved. On the other hand, the stabilization is important in the fracture region, for which we take

$$L_i = a(i, \varphi^{i-1})L_{i-1}, \qquad \text{with } a(i, \varphi^{i-1}) := (1 - \varphi^{i-1})a.$$

Recalling that the fracture is characterised by $\varphi \approx 0$, it becomes clear that the stabilization parameters are acting mainly in the fracture region. Finally, to improve further the convergence behaviour of the scheme we adapt Ξ at each iteration. In this case we take $\Xi_i = \Xi_{i-1} + \gamma[\varphi^{i-1} - \bar{\varphi}]^+$.

Algorithm 1 Dynamic variant of the L-scheme for a phase-field fracture

Choose $\gamma > 0$, $a > 1$, as well as Ξ^0 and L_0. Set $i = 0$.
repeat
  Let $i = i + 1$;
  Solve the two problems, namely
    Solve the nonlinear elasticity problem in (1)
    Solve the nonlinear phase-field problem in (2)
  Update $L^i = aL^{i-1}$
  Update $\Xi^i = \Xi^{i-1} + \gamma[\varphi^i - \bar{\varphi}]^+$
until
  $\max\{\|a_u(u^i, v)\|, \|a_\varphi(\varphi^i, \psi)\| / v \in V, \psi \in W\} \leq \text{TOL}$,

The final algorithm: The algorithm is based on the iterative procedure for phase-field fracture originally proposed in [9]. Therein, the inequality constraint is realized by an augmented Lagrangian iteration. Within this loop we update the L scheme parameters too. The resulting is sketched in Algorithm 3, in which $\text{TOL} = 10^{-6}$ is taken, and $L = L_u = L_\varphi$.

Remark 1 For the solution of both nonlinear subproblems (1) and (2), we use a monotonicity-based Newton method (details see e.g., in [10]) with the tolerance 10^{-8}. Inside Newton's method, we solve the linear systems with a direct solver.

4 Numerical tests

We consider two test examples. Details for the first test van be found in [7]. The setup of the second test can be found for instance in [6]. Both examples were already computed in [3] and the results therein are compared to the ones obtained here. The scheme is implemented in a code based on the deal.II library [2].

Single edge notched shear test: The configuration is shown in Figure 1. Specifically, we use $\mu_s = 80.77\,\text{kN/mm}^2$, $\lambda_s = 121.15\,\text{kN/mm}^2$, and $G_c = 2.7\,\text{N/mm}$. The crack growth is driven by a non-homogeneous Dirichlet condition for the displacement field on Γ_{top}, the top boundary of B . We increase the displacement on Γ_{top} over time, namely we apply non-homogeneous Dirichlet conditions:

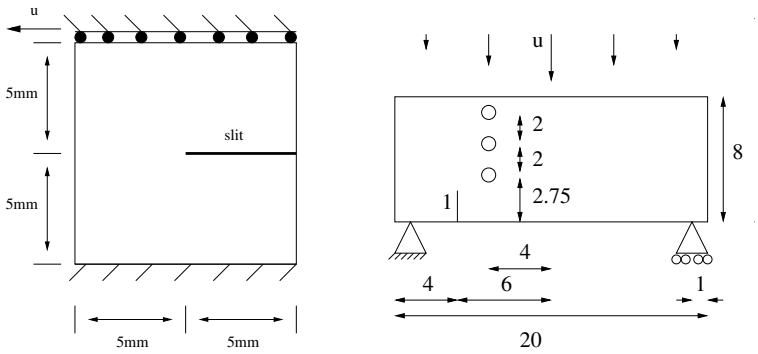

Fig. 1 Examples 1 and 2. The following conditions are prescribed: on the left and right boundaries, $u_y = 0\,\text{mm}$ and traction-free in x-direction. On the bottom part, $u_x = u_y = 0\,\text{mm}$. On Γ_{top}, $u_y = 0\,\text{mm}$ and u_x is as stated in (3). Finally, the lower part of the slit is fixed in y-direction, i.e., $u_y = 0\,\text{mm}$. Right: Asymmetric notched three point bending test. The three holes have each a diameter of 0.5. All units are in *mm*.

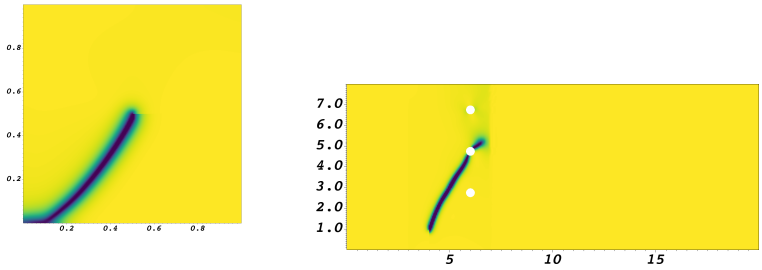

Fig. 2 Examples 1 and 2. Numerical solutions on the finest meshes and at the end time. The cracks are displayed in dark blue color.

$$u_x = t\bar{u}, \quad \bar{u} = 1\,\text{mm/s}, \tag{3}$$

where t denotes the current loading time. Furthermore, we set $\kappa = 10^{-10}$ [mm] and $\varepsilon = 2h$ [mm]. We evaluate the surface load vector on the Γ_{top} as

$$\tau = (F_x, F_y) := \int_{\Gamma_{\text{top}}} \boldsymbol{\sigma}(u)\nu \, \mathrm{d}s, \tag{4}$$

with normal vector ν, and we are particularly interested in the shear force F_x. Three different meshes with 1024 (Ref. 4), 4096 (Ref. 5) and 16384 (Ref. 6) elements are observed in order to show the robustness of the proposed schemes. The results are shown in Figure 6.

Our findings are summarized in Figure 3. The numerical solutions for all four different strategies for choosing L are practically identical, only the number of iterations being different. Here, $L = 0$ and $L = 1e-2$ denote tests in which $L = L_u = L_\varphi$ are taken constant throughout the entire computation. The newly

proposed dynamic versions are denoted by `L dynamic` and `L dyn. weighted`. We observe a significant reduction in the computational cost when using the dynamic L-schemes. The maximum number of iterations is 21 for both the weighted version and the spatially-constant L-scheme. This number is reduced to 12 iterations using $a = 20$ while the accuracy only slightly changes.

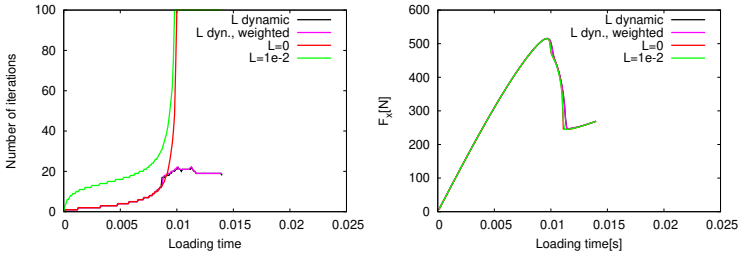

Fig. 3 Example 1. Comparison of dynamic L updates, the weighted version, and constant L. Left: number of iterations. Right: load-displacement curves.

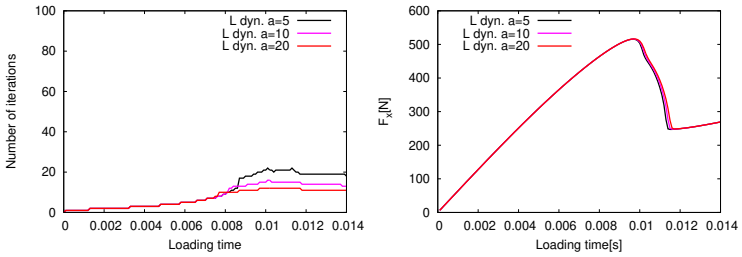

Fig. 4 Example 1. Comparison of different a for the dynamic L scheme.

Asymmetrically notched three point bending test: The configuration is shown in Figure 1 (right). The initial mesh is 3, 4 and 5 times uniformly refined, yielding 3 904, 15 616 and 62 464 mesh elements with the minimal mesh size parameter $h_3 = 0.135, h_4 = 0.066$ and $h_5 = 0.033$. As material parameters, we use $\mu_s = 8\,\mathrm{kN/mm^2}$, $\lambda_s = 12\,\mathrm{kN/mm^2}$, and $G_c = 1 \times 10^{-3}\,\mathrm{kN/mm}$. Furthermore, we set $k = 10^{-10}h[\mathrm{mm}]$ and $\varepsilon = 2h$.

Figure 5 presents the number of iterations and the load-displacement curves. The number of iterations is decreasing from 500 (in the figures cut to 100) for the classical L-scheme, to a maximum of 25 when using the dynamic updates. The choice of weighting does not seem to have a significant influence on the number of iterations though. The crack starts growing a bit later when using the dynamic updates, which can be inferred from the right plot in Figure 5. Thus, the stabilization parameters have a slight influence on the physical solution. This can be explained in the following way. In regions where $\varphi = 0$ the solution component u is not uniquely defined. This leads to a sub-optimal convergence behaviour of the L-scheme. With the dynamic L-scheme we regain uniqueness, but at the cost of a slightly modified physical problem.

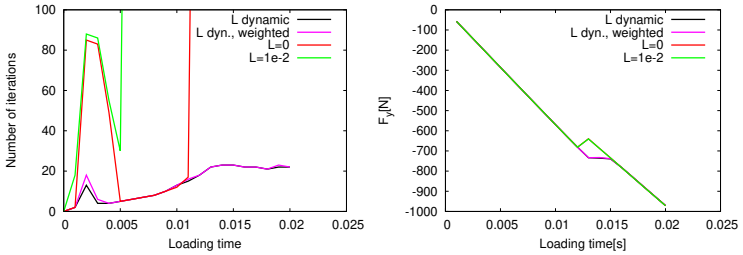

Fig. 5 Example 2: Left: The number of iterations for the different schemes; the results for $L = 0$ and $L = 1e-2$ are taken from [3]. Right: The load-displacement curves; a slight difference can be observed in the results, indicating that the dynamic updates lead to a slight delay in the prediction of the starting time for the fracture growth.

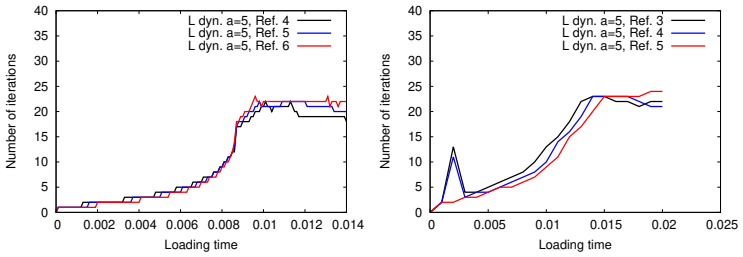

Fig. 6 Examples 1 and 2 for the dynamic L scheme using $a = 5$; three different mesh levels are used in order to verify the robustness of the proposed scheme. The results indicate that the mesh size does not influence the number of the iterations.

Remark 2 Noteworthy, the number of iterations for the dynamic L-scheme is robust with respect to the mesh refinement, as shown in Figure 6. This is in line with the analysis in [3, 5, 8], where it is proved that the convergence rate does not depend on the spatial discretization.

Acknowledgements

TW is supported by the German Research Foundation, Priority Program 1748 (DFG SPP 1748) under the project No. 392587580. CE is supported by the German Research Foundation, via Priority Program 1648 (DFG SPP 1648) under the grant No. EN-1042/2-2 and via EXC 2044-390685587, Mathematics Münster: Dynamics-Geometry-Structure. ISP is supported by the Research Foundation-Flanders (FWO), Belgium through the Odysseus programme (project G0G1316N).

References

1. E. L. Allgower and K. Georg. *Numerical continuation methods: an introduction*. Springer, 1990.
2. D. Arndt, W. Bangerth, T. C. Clevenger, D. Davydov, M. Fehling, D. Garcia-Sanchez, G. Harper, T. Heister, L. Heltai, M. Kronbichler, R. M. Kynch, M. Maier, J.-P. Pelteret, B. Turcksin, and D. Wells. The `deal.II` library, version 9.1. *J. Numer. Math.*, 2019. accepted.
3. M. K. Brun, T. Wick, I. Berre, J. M. Nordbotten, and F. A. Radu. An iterative staggered scheme for phase field brittle fracture propagation with stabilizing parameters. arXiv preprint arXiv:1903.08717, accepted for publication in Comp. Meth. Appl. Mech. Engrg., 2019.
4. T. Gerasimov and L. D. Lorenzis. A line search assisted monolithic approach for phase-field computing of brittle fracture. *Comp. Meth. Appl. Mech. Engrg.*, 312:276 – 303, 2016.
5. F. List and F. A. Radu. A study on iterative methods for solving Richards' equation. *Comput. Geosci.*, 20(2):341–353, 2016.
6. A. Mesgarnejad, B. Bourdin, and M. Khonsari. Validation simulations for the variational approach to fracture. *Comp. Meth. Appl. Mech. Engrg.*, 290:420 – 437, 2015.
7. C. Miehe, F. Welschinger, and M. Hofacker. Thermodynamically consistent phase-field models of fracture: variational principles and multi-field fe implementations. *Int. J. Numer. Methods Engrg.*, 83:1273–1311, 2010.
8. I. S. Pop, F. Radu, and P. Knabner. Mixed finite elements for the Richards' equation: linearization procedure. *J. Comput. Appl. Math.*, 168(1-2):365–373, 2004.
9. M. Wheeler, T. Wick, and W. Wollner. An augmented-Lagangrian method for the phase-field approach for pressurized fractures. *Comp. Meth. Appl. Mech. Engrg.*, 271:69–85, 2014.
10. T. Wick. An error-oriented Newton/inexact augmented Lagrangian approach for fully monolithic phase-field fracture propagation. *SIAM J. Sci. Comput.*, 39(4):B589–B617, 2017.

UHasselt Computational Mathematics Preprint Series

2019

UP-19-13 *C. Engwer, I.S. Pop, T. Wick*, **Dynamic and weighted stabilizations of the L-scheme applied to a phase-field model for fracture propagation**, 2019

UP-19-12 *M. Gahn*, **Singular limit for quasi-linear diffusive transport through a thin heterogeneous layer**, 2019

UP-19-11 *M. Gahn, W. Jäger, M. Neuss-Radu*, **Correctors and error estimates for reaction-diffusion processes through thin heterogeneous layers in case of homogenized equations with interface diffusion**, 2019

UP-19-10 *V. Kučera, M. Lukáčová-Medvidová, S. Noelle, J. Schütz,*, **Asymptotic properties of a class of linearly implicit schemes for weakly compressible Euler equations**, 2019

UP-19-09 *D. Seal, J. Schütz*, **An asymptotic preserving semi-implicit multiderivative solver**, 2019

UP-19-08 *H. Hajibeygi, M. Bastidas Olivares, M. HosseiniMehr, I.S. Pop, M.F. Wheeler*, **A benchmark study of the multiscale and homogenization methods for fully implicit multiphase ow simulations with adaptive dynamic mesh (ADM)**, 2019

UP-19-07 *J.W. Both, I.S. Pop, I. Yotov*, **Global existence of a weak solution to unsaturated poroelasticity**, 2019

UP-19-06 *K. Mitra, T. Köppl, I.S. Pop, C.J. van Duijn, R. Helmig*, **Fronts in two-phase porous flow problems: effects of hysteresis and dynamic capillarity**, 2019

UP-19-05 *D. Illiano, I.S. Pop, F.A. Radu*, **Iterative schemes for surfactant transport in porous media**, 2019

UP-19-04 *M. Bastidas, C. Bringedal, I.S. Pop, F.A. Radu*, **Adaptive numerical homogenization of nonlinear diffusion problems**, 2019

UP-19-03 *K. Kumar, F. List, I.S. Pop, F.A. Radu*, **Formal upscaling and numerical validation of fractured flow models for Richards' equation**, 2019

UP-19-02 *M.A. Endo Kokubun, A. Muntean, F.A. Radu, K. Kumar, I.S. Pop, E. Keilegavlen, K. Spildo*, **A pore-scale study of transport of inertial particles by water in porous media**, 2019

UP-19-01 *Carina Bringedal, Lars von Wolff, and Iuliu Sorin Pop*, **Phase field modeling of precipitation and dissolution processes in porous media: Upscaling and numerical experiments**, 2019

2018

UP-18-09 *David Landa-Marbán, Gunhild Bodtker, Kundan Kumar, Iuliu Sorin Pop, Florin Adrian Radu*, **An upscaled model for permeable biofilm in a thin channel and tube**, 2018

UP-18-08 *Vo Anh Khoa, Le Thi Phuong Ngoc, Nguyen Thanh Long*, **Existence, blow-up and exponential decay of solutions for a porous-elastic system with damping and source terms**, 2018

UP-18-07 *Vo Anh Khoa, Tran The Hung, Daniel Lesnic*, **Uniqueness result for an age-dependent reaction-diffusion problem**, 2018

UP-18-06 *Koondanibha Mitra, Iuliu Sorin Pop*, **A modified L-Scheme to solve nonlinear diffusion problems**, 2018

UP-18-05 *David Landa-Marban, Na Liu, Iuliu Sorin Pop, Kundan Kumar, Per Pettersson, Gunhild Bodtker, Tormod Skauge, Florin A. Radu*, **A pore-scale model for permeable biofilm: numerical simulations and laboratory experiments**, 2018

UP-18-04 *Florian List, Kundan Kumar, Iuliu Sorin Pop and Florin A. Radu*, **Rigorous upscaling of unsaturated flow in fractured porous media**, 2018

UP-18-03 *Koondanibha Mitra, Hans van Duijn*, **Wetting fronts in unsaturated porous media: the combined case of hysteresis and dynamic capillary**, 2018

UP-18-02 *Xiulei Cao, Koondanibha Mitra*, **Error estimates for a mixed finite element discretization of a two-phase porous media flow model with dynamic capillarity**, 2018

UP-18-01 *Klaus Kaiser, Jonas Zeifang, Jochen Schütz, Andrea Beck and Claus-Dieter Munz*, **Comparison of different splitting techniques for the isentropic Euler equations**, 2018

2017

UP-17-12 *Carina Bringedal, Tor Eldevik, Øystein Skagseth and Michael A. Spall*, **Structure and forcing of observed exchanges across the Greenland-Scotland Ridge**, 2017

UP-17-11 *Jakub Wiktor Both, Kundan Kumar, Jan Martin Nordbotten, Iuliu Sorin Pop and Florin Adrian Radu*, **Linear iterative schemes for doubly degenerate parabolic equations**, 2017

UP-17-10 *Carina Bringedal and Kundan Kumar*, **Effective behavior near clogging in upscaled equations for non-isothermal reactive porous media flow**, 2017

UP-17-09 *Alexander Jaust, Balthasar Reuter, Vadym Aizinger, Jochen Schütz and Peter Knabner*, **FESTUNG: A MATLAB / GNU Octave toolbox for the discontinuous Galerkin method. Part III: Hybridized discontinuous Galerkin (HDG) formulation**, 2017

UP-17-08 *David Seus, Koondanibha Mitra, Iuliu Sorin Pop, Florin Adrian Radu and Christian Rohde*, **A linear domain decomposition method for partially saturated flow in porous media**, 2017

UP-17-07 *Klaus Kaiser and Jochen Schütz*, **Asymptotic Error Analysis of an IMEX Runge-Kutta method**, 2017

UP-17-06 *Hans van Duijn, Koondanibha Mitra and Iuliu Sorin Pop*, **Travelling wave solutions for the Richards equation incorporating non-equilibrium effects in the capillarity pressure**, 2017

UP-17-05 *Hans van Duijn and Koondanibha Mitra*, **Hysteresis and Horizontal Redistribution in Porous Media**, 2017

UP-17-04 *Jonas Zeifang, Klaus Kaiser, Andrea Beck, Jochen Schütz and Claus-Dieter Munz*, **Efficient high-order discontinuous Galerkin computations of low Mach number flows**, 2017

UP-17-03 *Maikel Bosschaert, Sebastiaan Janssens and Yuri Kuznetsov*, **Switching to nonhyperbolic cycles from codim-2 bifurcations of equilibria in DDEs**, 2017

UP-17-02 *Jochen Schütz, David C. Seal and Alexander Jaust*, **Implicit multiderivative collocation solvers for linear partial differential equations with discontinuous Galerkin spatial discretizations**, 2017

UP-17-01 *Alexander Jaust and Jochen Schütz*, **General linear methods for time-dependent PDEs**, 2017

2016

UP-16-06 *Klaus Kaiser and Jochen Schütz*, **A high-order method for weakly compressible flows**, 2016

UP-16-05 *Stefan Karpinski, Iuliu Sorin Pop, Florin A. Radu*, **A hierarchical scale separation approach for the hybridized discontinuous Galerkin method**, 2016

UP-16-04 *Florin A. Radu, Kundan Kumar, Jan Martin Nordbotten, Iuliu Sorin Pop*, **Analysis of a linearization scheme for an interior penalty discontinuous Galerkin method for two phase flow in porous media with dynamic capillarity effects** , 2016

UP-16-03 *Sergey Alyaev, Eirik Keilegavlen, Jan Martin Nordbotten, Iuliu Sorin Pop*, **Fractal structures in freezing brine**, 2016

UP-16-02 *Klaus Kaiser, Jochen Schütz, Ruth Schöbel and Sebastian Noelle*, **A new stable splitting for the isentropic Euler equations**, 2016

UP-16-01 *Jochen Schütz and Vadym Aizinger*, **A hierarchical scale separation approach for the hybridized discontinuous Galerkin method**, 2016